

ZnO Binary and Ternary Composites

Subjects: **Nanoscience & Nanotechnology**

Contributor: Vu Khac Hoang Bui

ZnO is a promising anode candidate for LIBs owing to its high theoretical capacity (978 mAh g⁻¹). However, because of its limitations, such as its slow chemical reaction kinetics, rapid capacity fading, and poor rate capability, composites of ZnO must be formed with other materials. The highlighted studies on ZnO-based binary and ternary composites as anode for LIBs with different synthesis methods are summarized.

ZnO

composites

binary

ternary

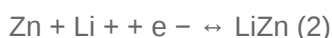
LIBs

anode

1. Introduction

Rechargeable lithium-ion batteries (LIBs) are widely used owing to their high specific energy, high electrochemical performance, and extended lifetime [1]. They are extensively adopted to power various electronic appliances, such as laptops and mobile phones. However, graphite, which is used as an anode in LIBs, limits their practical applications because of its low theoretical capacity (372 mAh g⁻¹) [2]. Semiconductor metal oxides (MOs) have the potential to enhance the performance of LIBs because of their higher theoretical capacity and safety than the traditional materials, such as carbon materials [3]. In the past ten years, the literature and patents on MOs and their composites for LIB applications have drastically increased, which is a trend that is expected to continue. Among MOs, zinc oxide (ZnO) (978 mAh g⁻¹) has an excellent theoretical capacity, which is only slightly lower than that of ferric oxide (Fe 2O₃). Compared to other MOs, ZnO not only has a higher theoretical capacity but also a lower cost, ease of synthesis, various synthesis methods, chemical stability, and different morphologies [4]. Therefore, in this study, ZnO-based composites were selected as the target.

As mentioned above, ZnO is a promising anode material candidate for LIBs owing to its high theoretical capacity (978 mAh g⁻¹) [5]. ZnO is a low-band gap semiconductor (3.37 eV) with unique properties such as a high exciton binding energy (60 meV), photoelectric response, and electron mobility. The above features along with its good thermal and chemical stability render ZnO useful for various applications [6]. The general electrochemical mechanism for a ZnO anode in an LIB is as follows [7]:



Equation (1) is a conversion reaction, and (2) is an alloying–dealloying reaction. In (1), ZnO captures more lithium ions (Li⁺) than traditional anodes, which proves beneficial during (2) [7]. Materials that undergo both conversion

and alloying–dealloying reactions have higher capacities than those that involve only alloying reactions [8]. Unlike tin oxide (SnO₂), which undergoes irreversible conversion and reversible alloying–dealloying reactions [9], for ZnO, both reactions are reversible [7][10].

However, ZnO has numerous limitations such as its slow chemical reaction kinetics, intense capacity fading on potential cycling, and low rate capability [11]. Moreover, it tends to aggregate and undergo a remarkable volume change (228%) during the charge/discharge cycles [7][12]. Although a thin layer formation occurs during the first cycle, it is extremely thin to be robust to the volume variation in ZnO. Thus, nanocracks can form inside ZnO and lead to continuous growth of the solid electrolyte interface (SEI) layer [13][14]. To realize LIB anodes with high reversible capacity, structural stability, and activity, materials with high conductivity are necessary [5].

Some strategies to increase the electrochemical performance of ZnO are to realize nanoscale-sized particles and to fabricate different nanoarchitectures, such as nanospheres, nanorods, nanotubes, and nanosheets [15][16][17][18]. Nanostructured MOs can decrease the Li⁺ diffusion time and enhance the rate performance [9]. ZnO nanoarchitectures not only provide a barrier against the volume variation during the cycling process but also enhance the electrode/electrolyte contact area [19]. However, such different nanosized and morphological ZnO forms still have a low intrinsic electrical conductivity and exhibit a large volume change during the charge/discharge process [20]. Concurrently, composites of ZnO and other materials can be formed to increase its initial capacity and decrease the degradation during the charge/discharge process [7]. In addition, coating ZnO on materials such as carbon can alleviate the volume change problem [7][21]. Thus, ZnO-based nanomaterials offer a high electrochemical conductivity, a short transport path for Li⁺, and an extended lifetime [7]. In this entry, we focus on ZnO-based binary and ternary composites.

2. ZnO Binary Composites

Although the CV curves of the intermixed and nanolaminated ZnO–SnO₂ composites were similar, in the cathodic scan, the latter showed a lower reversibility than the former. Compare to single ZnO and SnO₂ anodes, both intermixed and nanolaminated ZnO–SnO₂ composites have a higher capacity and initial Coulombic efficiency (CE). The first discharge capacity and Coulombic efficiency (CE) of the intermixed ZnO–SnO₂ were 2667 mAh g⁻¹ and 80.2%, respectively, and for the nanolaminated ZnO–SnO₂, these were 2471 mAh g⁻¹ and 71.4%, respectively. The higher CE indicated that intermixed ZnO–SnO₂ is more reversible. Both the intermixed and nanolaminated ZnO–SnO₂ composites presented a better cycling stability than pure SnO₂ and ZnO. For the nanolaminated composite, a capacity decrease occurred only after the 35th cycle. In comparison, the capacity of the intermixed composite was initially stable until the 10th cycle, subsequently increased to 1752 mAh g⁻¹, and remained almost constant up to the 50th cycle. After the 50th cycle, particle expansion occurred in the intermixed ZnO–SnO₂ electrode without disruption of their interconnections, resulting in a surface with fewer crevasses and more cycling stability than the nanolaminated composite surface. At the atomic scale, when mixing ZnO and SnO₂, ZnO reduction suppresses the alloying of Sn, and the produced reduced Zn⁰ also assists SnO₂, which improves the morphological stability of the anode during the cycling process and increases its cyclability. For the nanolaminated composite, the interface formation between ZnO and SnO₂ leads to isolation intercalation and

alloying reactions with the injected lithium, resulting in a severe volume change, specifically in the latter reaction. Moreover, the conductivity of the intermixed composite was improved. In view of these results, Zhao et al. (2019) explored the atomic ratio effect on the electrochemical properties of intermixed composites. For intermixed $\text{ZnO}-2\text{SnO}_2$ composites containing ZnO and SnO_2 in a 1:2 atomic ratio, the discharge capacities in the first, second, and thirtieth cycles were 2637, 2230, and 1771 mAh g^{-1} , respectively, and the initial CE was 84.5%. The corresponding capacities for intermixed $2\text{ZnO}-\text{SnO}_2$ composites with ZnO and SnO_2 in a 2:1 atomic ratio were 2495, 2018, and 1492 mAh g^{-1} , and the first cycle CE was 80.9%. Both the $\text{ZnO}-2\text{SnO}_2$ and $2\text{ZnO}-\text{SnO}_2$ composites had high cyclabilities of 1955 and 1794 mAh g^{-1} at 0.5 A g^{-1} after 50 cycles, respectively. It was concluded that the change in the atomic ratio did not significantly affect the electrochemical activity of these intermixed composites. Although the capacity could be tuned by changing the atomic ratio, the rate and cycling performance were minor. Interestingly, annealing the $\text{ZnO}-\text{SnO}_2$ composite film in ambient helium at 1000 °C for 2 h led to the formation of a Zn_2SnO_4 film, making the surface of the annealed composite rough with some pinholes. The first and second discharge capacities of the Zn_2SnO_4 film were 2363 and 1915 mAh g^{-1} , its CE was 81% after the first cycle, and its capacity remained ~ 1515 mAh g^{-1} at 0.5 A g^{-1} after 50 cycles. As the current density was increased in the order 0.5, 0.8, 1, 2, and 5 A g^{-1} , the discharge capacity decreased in sequence as 1652, 1331, 1074, 818, and 514 mAh g^{-1} . When the current density was reduced to 0.5 A g^{-1} again, the discharge capacity increased to reach 1448 mAh g^{-1} , indicating the good rate capability of the Zn_2SnO_4 film. Thus, annealing did not have a significant influence on the electrochemical potential. Therefore, the most influencing factor of the electrochemical performance of $\text{ZnO}-\text{SnO}_2$ composites is the degree of mixing, and not the crystallinity degree or the exact composition [6].

Owing to its nanoporous structure, good conductive network, and strain accommodation, PC has been utilized as a dispersion medium for many MOs, such as ZnO , SnO_2 , TiO_2 , and Fe_3O_4 [5][22][23]. It protects MOs from aggregation and pulverization [5]. Shen et al. (2013) prepared ZnO/PC composites using the solvothermal method. The first discharge/charge capacity of ZnO (54 wt%)/PC was 2017.4/1062.9 mAh g^{-1} (CE: 52.68%), and it had a high reversible capacity of 653.7 mAh g^{-1} at 0.1 A g^{-1} after 100 cycles. The high lithium storage potential of this ZnO/PC composite can be attributed to its nanoporous structure and interconnected network. Lowering the ZnO loading reduced the discharge capacity of the ZnO/PC composite, whereas increasing the ZnO loading blocked the PC pores. In addition, at a high ZnO loading, the increase in the ZnO particle size increased the mechanical stress in the composite. The morphology of pure ZnO severely deteriorated after the lithiation/delithiation cycling, which led to a low reversible capacity. In contrast, the ZnO/PC composite maintained its original morphology without significant pulverization or cracks after the charge/discharge cycles. It can be concluded that the PC host provided space for the volume variation in the ZnO particles during the intercalation/deintercalation process, thereby preventing electrode degradation [5].

Coating carbon on ZnO leads to rapid electron mobility over its entire surface during cycling, thus enhancing the reversibility and kinetics of the Li^+ insertion/extraction [24][25]. Carbon coating also protects MOs from dissolving in the electrolyte, protects composite deformation, and maintains high conductivity [7][26]. In 2016, Quartarone et al. synthesized graphite-coated ZnO nanosheets as binder-free anodes for LIBs. The ZnO nanosheets were prepared by the hydrothermal process and coated with graphite by thermal evaporation. The graphite-coated ZnO nanosheet

composite having a graphite thickness of 350 Å presented the first discharge/charge capacity of 1470/968 mAh g⁻¹ (CE: 65.85%) and a specific capacity of 600 mAh g⁻¹ after 100 cycles at 1 A g⁻¹. The specific capacity of the uncoated ZnO nanosheet was 400 mAh g⁻¹ at 1 A g⁻¹ after 100 cycles. The formation of micropores (pore diameter < 1 nm) within the composite and the enhancement of the exposed surface area were ascribed to the ZnO NPs' nucleation. The ZnO NPs were 15 nm in size, and the nanosheet width and length were approximately 0.8–1.5 μm. The small sizes of the ZnO NPs and their nanostructure not only increased the electrode/electrolyte contact area and the electrical contact but also achieved high strain accommodation. Concurrently, the graphite coating acted as a buffer against the change in the composite morphology during the charge/discharge process [27].

Gan et al. (2017) prepared N-doped carbon-coated ZnO nanorods (ZnO/NC-Z NRDs) using a solvent-free method as anodes for LIBs. N-doped carbon was synthesized by thermal treatment of zeolitic imidazolate framework-8 (ZIF-8), which was previously in situ grown on ZnO NRD surfaces. The study claimed that by using the in situ strategy, the adhesive force from the interaction between the carbon and ZnO NRDs was stronger than that with conventional ex situ methods, which resulted in a limited confinement effect in the latter [20]. Thus, compared to conventional ex situ methods, in situ methods realized a tighter coating of carbon on the ZnO NRD surfaces. TEM results showed that the carbon layer thickness was approximately 15–20 nm. Based on the XRD patterns, ZIF-8 was completely converted into amorphous carbon and ZnO after carbonization in Ar atmosphere. From the XPS analysis, the nitrogen concentration in the ZnO/NC-Z NRDs was approximately 2.3% and considered to enhance the composite electrical conductivity [20]. The carbon prepared from ZIF-8 exhibited specific properties such as a large surface area, tunable porosity, and structural stability and flexibility [20]. Owing to these characteristics, ZIF-8 can be employed in different energy storage systems, including supercapacitors, LIBs, and sodium-ion batteries [28] [29] [30] [31]. Similar to the abovementioned carbon-based materials, N-doped carbon increased the NRD conductivity and, consequently, enhanced the Li⁺ diffusion rate. It also acted as a buffer layer, alleviating the volume variation during the cycling process. ZnO/ NC-Z NRDs had a specific BET surface area of 135.9 m² g⁻¹ (higher than ZnO NRDs, 47.9 m² g⁻¹) and a mesoporous structure (pore size of 3.85–5.53 nm). The presence of N-doped carbon also increased the ZnO/NC-Z NRD pore volume. The enhancements in the SSA and pore volume can be attributed to the decomposition of the ZIF-8 framework during the sintering process. The as-prepared composite had a capacity of 1439 mAh g⁻¹ at 0.2 A g⁻¹ and an initial CE of 76%; the latter was higher than that of the ZnO/C-P NRDs (71%) (sample prepared by ex situ method) and ZnO NRDs (67%). The higher CE of the ZnO/NC-Z NRD composite can be explained by the coated carbon layer preventing the detrimental reactions between the electrolyte and the ZnO NRDs. After 200 and 850 cycles, the capacity of the composite was reduced to 1011 mAh g⁻¹ at 0.2 A g⁻¹ and to 544 mAh g⁻¹ at 1 A g⁻¹ (capacity retention: 87.7%). The CE of the ZnO/NC-Z NRDs was found to be approximately 100% after the first cycle, indicating the ease of Li⁺ insertion/extraction and efficient electron and ion transfer. Using the four-point probe method showed that the electrical conductivity of the ZnO/NC-Z NRDs was higher than that of the ZnO/C-P NRDs and ZnO NRDs. After 150 cycles, the NRD morphology of the ZnO/NC-Z NRDs was preserved without any significant structural damage. The charge transfer resistance (R_(sf+ct)) of the ZnO/NC-Z NRDs (61 Ω) was lower than that of the ZnO/C-P NRDs (102 Ω) and ZnO NRDs (175 Ω). Moreover, the ZnO/NC-Z NRDs could be additionally used as precursors to synthesize N-doped

carbon nanotubes (CNTs), which had a capacity of $1001.1 \text{ mAh g}^{-1}$ after 100 cycles at 0.2 A g^{-1} and a capacity retention of 99.1% [20].

3. ZnO Ternary Composites

Besides binary composites, ternary composites have been investigated in different studies. Most of these ternary composites comprised ZnO, another MO, and PC-based materials. The synergistic effects between these materials can explain the improved electrochemical performance of the corresponding composites. For example, the PC materials serve as a buffer matrix to alleviate the volume expansion and capacity fading problems, whereas the ZnO and MO composite can protect the active materials from aggregation and enhance the electrode conductivity [32]. However, the electrochemical characteristics of ternary composites are less remarkable than those of the abovementioned binary composites.

Another ternary composite can be formed with ZnO and NiO. Similar to binary ZnO/MO and SnO₂/MO composites, the limitations of NiO/MO binary composites originate from their poor electronic conductivity and structural change during the repeated cycling, which result in a poor rate capability and rapid capacity fading. In 2018, Ma et al. prepared a NiO–ZnO/reduced graphene oxide (NiO–ZnO/RGO) composite by a process consisting of ultrasonic, freeze drying, and thermal treatments. The SEM results showed that the synthesized NiO–ZnO nanoflakes were uniformly distributed on the RGO sheet. The as-prepared electrodes had a first discharge capacity of 1393 mAh g^{-1} (CE: 66.3%) and high reversible capacities of 1017 mAh g^{-1} at 0.1 A g^{-1} after 200 cycles and 458 mAh g^{-1} at 0.5 A g^{-1} after 400 cycles. The reversible capacity of the ternary composite (1017 mAh g^{-1}) was higher than the theoretical capacity (833 mAh g^{-1}). After 15 cycles, the NiO–ZnO/RGO composite electrode had a higher CE (98%) than the NiO–ZnO hybrid anode. The reversible capacities of NiO and NiO–ZnO were reduced to 212 mAh g^{-1} at 180 cycles and 247 mAh g^{-1} at 150 cycles, respectively. The enhancement in the capacity of the NiO–ZnO/RGO composite was contributed by the formation of a reversible polymeric gel-like film with a high material viscosity provided by ZnO, which enhances the adhesion between the active material layer and the current collector [33]. NiO–ZnO/RGO had a smaller charge transfer resistance than the NiO–ZnO binary composite. Similar to MWCNTs and other carbon-based materials, the RGO prevents NiO–ZnO agglomeration and the volume variation during the charge/discharge cycles. NiO–ZnO nanoflakes were considered to provide abundant electrochemical reaction sites and decrease the Li^+ diffusion length, whereas the role of RGO was to enhance the Li^+ and electron transfer rates during the cycling process [34]. In the above study, the synergistic effect between NiO–ZnO and RGO was similar to that in the abovementioned binary composites. However, the combination effects of NiO and ZnO were not clearly explained.

Germanium oxide (GeO₂) is a promising anode material because of its high theoretical reversible capacity (1125 mAh g^{-1}), low operating voltage, and good thermal stability [35][36][37]. He et al. (2019) reported freestanding mesoporous foldable GeO_x/ZnO/C (FGCZ) composite nanofibers with uniform distributions of GeO_x and ZnO. A solution of polyacrylonitrile (PAN), zinc acetate (Zn(Ac)₂), CNTs, and GeO₂ NPs was used to fabricate nanofibers by electrospinning. The precursor nanofibers were stabilized by 2 h of annealing in air at 250°C and were subsequently carbonized by 6 h of annealing in air at 700°C to yield the FGCZ nanofibers. The resulting

nanofibers possessed uniform diameters of approximately 300 nm, longer than those of the GeO_x sample. The above can be explained based on the presence of Zn(Ac)₂ causing plasticization of PAN via the formation of N–Zn coordinative bonds. XPS analysis confirmed the existence of Ge₂O₃, formed by the reduction of GeO₂ by carbon at 700 °C, as well as ZnO in the composite fibers. Raman spectra, via I D / I G, indicated FGCZ was more disordered than GC (the sample prepared in the absence of Zn(Ac)₂) owing to the presence of Zn(Ac)₂. FGCZ also had a larger surface area (532.56 m² g⁻¹) than GC (236.33 m² g⁻¹). Mesopores with widths of 4–7 nm were also found in FGCZ, whose highly porous structure enhanced the electron transmission, provided more Li storage sites, and increased the rate of Li ion transport, thus improving the electrochemical performance. In their study, besides serving as the ZnO precursor and promoting the formation of mesopores, the added Zn(Ac)₂ in the electrospun solution achieved the following: (i) enhancement in the mechanical properties and flexibility of the composites, and (ii) assisting in the dispersion of GeO₂ NPs. Thus, the as-prepared FGCZ composite presented good electrochemical characteristics with a first discharge/charge capacity of 1000/890 mAh g⁻¹ at 0.2 A g⁻¹ (CE: 66.9%). After the 200th cycle at 0.2 A g⁻¹ and 500th cycle at 1 A g⁻¹, the FGCZ composite achieved discharge capacities of 617 and 464 mAh g⁻¹, respectively. Owing to the presence of amorphous active materials, their uniform dispersion, and the good conductivity of CNTs, the FGCZ composite showed rapid Li ion diffusion and therefore exhibited higher reversible capacities than the GC sample at the same high current density. When the FGCZ composite was assembled into full cells using a commercial flexible LiCoO₂/CNT as the cathode, it displayed a discharge capacity of 417 mAh g⁻¹ at 0.1 A g⁻¹. A ten-fold bent full battery had a discharge capacity of 391 mAh g⁻¹, which confirmed the good mechanical stability of the FGCZ composite. He et al. (2019) found that their full battery with FGCZ powered a light-emitting diode under different bending conditions. Specifically, under different bending angles, there was no significant difference in the EIS plots of the FGCZ composite [38].

Similar to ZnCo₂O₄, Ma et al. (2017) introduced ZnO/ZnFe₂O₄/N-doped C-micro-polyhedra (ZZFO-C) as anodes for LIBs. The composites were prepared by thermal treatment of ZIF–ZnFe (molar ratio of 3:1) for 2 h at 500 °C. XRD results confirmed the co-existence of ZnFe₂O₄ and ZnO. XPS analysis identified various nitrogen-doped carbon species and oxygen functional groups. The ZZFO-C composites had an average size of ~420 nm, slightly smaller than that of the ZIF–ZnFe precursor, owing to the partial framework decomposition and contraction throughout the calcination. The ZZFO-C composites possessed rougher surfaces than their precursors and comprised clustered MOs/carbon NPs (size of ~20 nm) and many small holes. The formation of the hollow structure is a consequence of the decomposition of the inner ZIF–ZnFe to form gaseous products, such as CO₂, H₂O, and NO₂ [39][40][41][42][43]. The ZnO/ZnFe₂O₄ NPs and the carbon layers overlapped with each other in the composite. Ma et al. (2017) found that when the annealing temperature was increased to 650 °C, the carbon in the composite was removed (noted as ZZFO). The surface area and pore size of ZZFO-C were 84.3 m² g⁻¹ and 13 nm, respectively, and for ZZFO, they were 31.2 m² g⁻¹ and 39 nm, respectively. The mesoporous structures of ZZFO-C and ZZFO were beneficial for the Li⁺ transport and could alleviate the volume change during insertion/desertion cycles. In terms of the electrochemical performance, ZZFO-C had a first discharge capacity of 1751 mAh g⁻¹ (CE: 67.4%). The higher CE of ZZFO-C than that of ZZFO (60.8%) can be explained by the presence of the N-doped carbon matrix, which improves the reversibility of the electrode. After 100 cycles at 0.2 A

g^{-1} and 2.0 A g^{-1} , the obtained ZZFO-C composite presented reversible capacities of 1000 mAh g^{-1} and 620 mAh g^{-1} , respectively. It also displayed a good rate capability with specific capacities of 1075, 1052, 1024, 928, 842, and 787 mAh g^{-1} at $0.05, 0.1, 0.2, 0.5, 1$, and 2 A g^{-1} , respectively. After returning to 0.1 A g^{-1} at the 75th cycle, the ZZFO-C composite recovered its initial specific capacity (1190 mAh g^{-1}), which continuously increased to reach 1328 mAh g^{-1} at the 90th cycle. Compared to ZZFO-C, the ZZFO sample showed poorer electrochemical activity. The good electrochemical performance of the ZZFO-C composite can be attributed to the synergistic effect between the N-doped carbon matrix and the two active components as well as its distinct hierarchical hollow structure [44].

4. Conclusions and Perspectives

ZnO is a promising anode candidate for LIBs owing to its high theoretical capacity (978 mAh g^{-1}) [5]. However, because of its limitations, such as its slow chemical reaction kinetics, rapid capacity fading, and poor rate capability [11], composites of ZnO must be formed with other materials. Most ZnO-based composites had higher first discharge capacities than only ZnO. Moreover, most of the composites discussed in this review showed a good cycling stability and rate performance. The large electrode/electrolyte contact area, abundant charge storage reaction sites, short Li^+ diffusion path, improved conductivity, stability structure, and potential to relieve the volume expansion could explain the good electrical performance of these anode composites. To synthesize high-performance anodes, different factors such as size, morphology, crystallinity, phase composition, and porosity should be considered [9]. Some limitations of ZnO-based composites have also been found and should be overcome rapidly. The synergistic effects between the components of the composites as well as the correlation between the composite structure and the electrical performance should be investigated in more detail. In general, the initial CEs of ZnO-based composites were low and should be increased, for which electrolyte optimization, surface modification, and coating of ZnO are possible solutions [9][45][46]. In the case of ZnO–MO binary composites, the choice of MO partner to prepare ZnO–MOs may increase the initial CE. Both conversion and alloying MOs can increase the capacity of composites. However, between reversible conversion and alloying–dealloying reactions, the reversible alloying–dealloying reaction may have more benefits in the increase in the initial CE. For example, the presence of alloying materials (SnO_2) in the composite can increase the initial CE, while the presence of conversion materials (NiO) has less impact on the improvement in the initial CE [6][47]. Moreover, the relationships between active materials, binders, and electrolyte additives should be further investigated in order to improve the SEI layer and thus result in a better CE and cycle performance [9]. Strategies to develop ZnO-based composites that have high energy densities should be identified. For example, in ZnO–carbon-based composites, the carbon component contributes slightly to the capacity but accounts for more than 50% of the total electrode weight. Therefore, the total energy density of these composites is significantly lowered, which reduces the potential of PC materials in real LIB applications. In addition, there are considerable efforts to synthesize ZnO ternary composites with different structures. However, their electrochemical performance is not significantly higher when compared to similar binary composite anodes for LIBs. For example, the ZnO/ SnO_2 /MWCNT and NiO–ZnO/RGO ternary composites mentioned in this paper did not have a better initial discharge capacity and cycling performance when compared to ZnO– SnO_2 and ZnO–NiO. In addition, most of the studies

mentioned in this review focused on developing composites with a high specific capacity instead of producing composites with a high packing density and a high energy density. Thus, we recommend aiming at generating novel composites or optimizing ZnO-based composites that not only have a high specific capacity, cycling stability, and rate performance but also a high initial CE and energy density. In this review, some studies such as Li et al. (ZnO–NiO microspheres, 2018) and Zhao et al. (C/ZnO NMs, 2018) focused on improvements not only in the electrochemical performance of their studied composites but also in their energy density [47][48]. Moreover, a more synthetic process than the current ones should be developed to reduce the production cost to meet industrial requirements.

References

1. Kang, S.; Li, Y.; Wu, M.; Cai, M.; Shen, P.K. Synthesis of hierarchically flower-like FeWO₄ as high performance anode materials for Li-ion batteries by a simple hydrothermal process. *Int. J. Hydrog. Energy* 2014, 39, 16081–16087.
2. Nguyen, Q.H.; Phung, V.D.; Kidanu, W.G.; Ahn, Y.N.; Nguyen, T.L.; Kim, I.T. Carbon-free Cu/SbxOy/Sb nanocomposites with yolk-shell and hollow structures as high-performance anodes for lithium-ion storage. *J. Alloys Compd.* 2021, 878, 160447.
3. Zhu, J.; Zhang, G.; Gu, S.; Lu, B. SnO₂ nanorods on ZnO nanofibers: A new class of hierarchical nanostructures enabled by electrospinning as anode material for high-performance lithium-ion batteries. *Electrochim. Acta* 2014, 150, 308–313.
4. Li, H.; Wei, Y.; Zhang, Y.; Yin, F.; Zhang, C.; Wang, G.; Bakenov, Z. Synthesis and electrochemical investigation of highly dispersed ZnO nanoparticles as anode material for lithium-ion batteries. *Ionics* 2016, 22, 1387–1393.
5. Shen, X.; Mu, D.; Chen, S.; Wu, B.; Wu, F. Enhanced electrochemical performance of ZnO-loaded/porous carbon composite as anode materials for lithium ion batteries. *ACS Appl. Mater. Interfaces* 2013, 5, 3118–3125.
6. Zhao, B.; Mattelaer, F.; Kint, J.; Werbrouck, A.; Henderick, L.; Minjauw, M.; Dendooven, J.; Detavernier, C. Atomic layer deposition of ZnO–SnO₂ composite thin film: The influence of structure, composition and crystallinity on lithium-ion battery performance. *Electrochim. Acta* 2019, 320, 134604.
7. Zhang, J.; Gu, P.; Xu, J.; Xue, H.; Pang, H. High performance of electrochemical lithium storage batteries: ZnO-based nanomaterials for lithium-ion and lithium-sulfur batteries. *Nanoscale* 2016, 8, 18578–18595.
8. Aravindan, V.; Jinesh, K.B.; Prabhakar, R.R.; Kale, V.S.; Madhavi, S. Atomic layer deposited (ALD) SnO₂ anodes with exceptional cycleability for Li-ion batteries. *Nano Energy* 2013, 2, 720–

725.

9. Chen, Y.; Chen, X.; Zhang, Y. A Comprehensive Review on Metal-Oxide Nanocomposites for High-Performance Lithium-Ion Battery Anodes. *Energy Fuels* 2021, 35, 6420–6442.
10. Yuan, G.; Wang, G.; Wang, H.; Bai, J. Synthesis and electrochemical investigation of radial ZnO microparticles as anode materials for lithium-ion batteries. *Ionics* 2015, 21, 365–371.
11. Hsieh, C.T.; Lin, C.Y.; Chen, Y.F.; Lin, J.S. Synthesis of composites as anode materials for lithium ion batteries. *Electrochim. Acta* 2013, 111, 359–365.
12. Lu, S.; Wang, H.; Zhou, J.; Wu, X.; Qin, W. Atomic layer deposition of ZnO on carbon black as nanostructured anode materials for high-performance lithium-ion batteries. *Nanoscale* 2017, 9, 1184–1192.
13. Liu, N.; Lu, Z.; Zhao, J.; McDowell, M.T.; Lee, H.W.; Zhao, W.; Cui, Y. A pomegranate-inspired nanoscale design for large-volume-change lithium battery anodes. *Nat. Nanotechnol.* 2014, 9, 187–192.
14. Gao, H.; Zhou, W.; Jang, J.H.; Goodenough, J.B. Cross-Linked Chitosan as a Polymer Network Binder for an Antimony Anode in Sodium-Ion Batteries. *Adv. Energy Mater.* 2016, 6, 1502130.
15. Li, F.; Yang, L.; Xu, G.; Xiaoqiang, H.; Yang, X.; Wei, X.; Ren, Z.; Shen, G.; Han, G. Hydrothermal self-assembly of hierarchical flower-like ZnO nanospheres with nanosheets and their application in Li-ion batteries. *J. Alloys Compd.* 2013, 577, 663–668.
16. Park, K.T.; Xia, F.; Kim, S.W.; Kim, S.B.; Song, T.; Paik, U.; Park, W.I. Facile synthesis of ultrathin ZnO nanotubes with well-organized hexagonal nanowalls and sealed layouts: Applications for lithium ion battery anodes. *J. Phys. Chem. C* 2013, 117, 1037–1043.
17. Huang, X.H.; Guo, R.Q.; Wu, J.B.; Zhang, P. Mesoporous ZnO nanosheets for lithium ion batteries. *Mater. Lett.* 2014, 122, 82–85.
18. Zhang, G.; Hou, S.; Zhang, H.; Zeng, W.; Yan, F.; Li, C.C.; Duan, H. High-performance and ultra-stable lithium-ion batteries based on MOF-derived quantum dots/C core-shell nanorod arrays on a carbon cloth anode. *Adv. Mater.* 2015, 27, 2400–2405.
19. Ge, X.; Li, Z.; Wang, C.; Yin, L. Metal-organic frameworks derived porous core/shell structured ZnO/ZnCo₂O₄/C hybrids as anodes for high-performance lithium-ion battery. *ACS Appl. Mater. Interfaces* 2015, 7, 26633–26642.
20. Gan, Q.; Zhao, K.; Liu, S.; He, Z. Solvent-free synthesis of N-doped carbon coated ZnO nanorods composite anode via a ZnO support-induced ZIF-8 in-situ growth strategy. *Electrochim. Acta* 2017, 250, 292–301.
21. Bresser, D.; Mueller, F.; Fiedler, M.; Krueger, S.; Kloepsch, R.; Baither, D.; Winter, M.; Paillard, E.; Passerini, S. Transition-metal-doped zinc oxide nanoparticles as a new lithium-ion anode

material. *Chem. Mater.* 2013, 25, 4977–4985.

22. Yu, Z.; Zhu, S.; Li, Y.; Liu, Q.; Feng, C.; Zhang, D. Synthesis of SnO₂ nanoparticles inside mesoporous carbon via a sonochemical method for highly reversible lithium batteries. *Mater. Lett.* 2011, 65, 3072–3075.

23. Liu, J.; Zhou, Y.; Liu, F.; Liu, C.; Wang, J.; Pan, Y.; Xue, D. One-pot synthesis of mesoporous interconnected carbon-encapsulated Fe₃O₄ nanospheres as superior anodes for Li-ion batteries. *RSC Adv.* 2012, 2, 2262–2265.

24. Wu, S.; Wang, W.; Li, M.; Cao, L.; Lyu, F.; Yang, M.; Wang, Z.; Shi, Y.; Nan, B.; Yu, S.; et al. Highly durable organic electrode for sodium-ion batteries via a stabilized α -C radical intermediate. *Nat. Commun.* 2016, 7, 1–11.

25. Wu, S.; Zhu, Y.; Huo, Y.; Luo, Y.; Zhang, L.; Wan, Y.; Nan, B.; Cao, L.; Wang, Z.; Li, M.; et al. Bimetallic organic frameworks derived CuNi/carbon nanocomposites as efficient electrocatalysts for oxygen reduction reaction. *Sci. China Mater.* 2017, 60, 654–663.

26. Duan, Z.Q.; Liu, Y.T.; Xie, X.M.; Ye, X.Y.; Zhu, X.D. H-BN Nanosheets as 2D Substrates to Load 0D Fe₃O₄ Nanoparticles: A Hybrid Anode Material for Lithium-Ion Batteries. *Chem. Asian J.* 2016, 11, 828–833.

27. Quartarone, E.; Dall’asta, V.; Resmini, A.; Tealdi, C.; Tredici, I.G.; Tamburini, U.A.; Mustarelli, P. Graphite-coated ZnO nanosheets as high-capacity, highly stable, and binder-free anodes for lithium-ion batteries. *J. Power Sources* 2016, 320, 314–321.

28. Li, Z.; Yin, L. Sandwich-like reduced graphene oxide wrapped MOF-derived ZnCo₂O₄-ZnO-C on nickel foam as anodes for high performance lithium ion batteries. *J. Mater. Chem. A* 2015, 3, 21569–21577.

29. Gan, Q.; Liu, S.; Zhao, K.; Wu, Y.; He, Z.; Zhou, Z. Graphene supported nitrogen-doped porous carbon nanosheets derived from zeolitic imidazolate framework for high performance supercapacitors. *RSC Adv.* 2016, 6, 78947–78953.

30. Li, C.; Hu, Q.; Li, Y.; Zhou, H.; Lv, Z.; Yang, X.; Liu, L.; Guo, H. Hierarchical hollow Fe₂O₃ @MIL-101(Fe)/C derived from metal-organic frameworks for superior sodium storage. *Sci. Rep.* 2016, 6, 1–8.

31. Yu, L.; Liu, J.; Xu, X.; Zhang, L.; Hu, R.; Liu, J.; Yang, L.; Zhu, M. Metal-organic framework-derived NiSb alloy embedded in carbon hollow spheres as superior lithium-ion battery anodes. *ACS Appl. Mater. Interfaces* 2017, 9, 2516–2525.

32. Köse, H.; Dombaycíoğlu, Ş.; Aydin, A.O.; Akbulut, H. Production and characterization of free-standing ZnO/SnO₂/MWCNT ternary nanocomposite Li-ion battery anode. *Int. J. Hydrog. Energy* 2016, 41, 9924–9932.

33. Qiao, L.; Wang, X.; Sun, X.; Li, X.; Zheng, Y.; He, D. Single electrospun porous NiO-ZnO hybrid nanofibers as anode materials for advanced lithium-ion batteries. *Nanoscale* 2013, 5, 3037–3042.

34. Ma, L.; Pei, X.Y.; Mo, D.C.; Lyu, S.S.; Fu, Y.X. Fabrication of NiO-ZnO/RGO composite as an anode material for lithium-ion batteries. *Ceram. Int.* 2018, 44, 22664–22670.

35. Wang, X.L.; Han, W.Q.; Chen, H.; Bai, J.; Tyson, T.A.; Yu, X.Q.; Wang, X.J.; Yang, X.Q. Amorphous hierarchical porous GeO_x as high-capacity anodes for Li ion batteries with very long cycling life. *J. Am. Chem. Soc.* 2011, 133, 20692–20695.

36. Jin, S.; Li, N.; Cui, H.; Wang, C. Growth of the vertically aligned amorphous GeO_x sandwich nanoflakes and excellent Li storage properties. *Nano Energy* 2013, 2, 1128–1136.

37. Medvedev, A.G.; Mikhaylov, A.A.; Grishanov, D.A.; Yu, D.Y.W.; Gun, J.; Sladkevich, S.; Lev, O.; Prikhodchenko, P.V. GeO₂ Thin Film Deposition on Graphene Oxide by the Hydrogen Peroxide Route: Evaluation for Lithium-Ion Battery Anode. *ACS Appl. Mater. Interfaces* 2017, 9, 9152–9160.

38. He, X.; Hu, Y.; Chen, R.; Shen, Z.; Wu, K.; Cheng, Z.; Pan, P. Foldable uniform GeO_x/ZnO/C composite nanofibers as a high-capacity anode material for flexible lithium ion batteries. *Chem. Eng. J.* 2019, 360, 1020–1029.

39. Zhang, L.; Wu, H.B.; Madhavi, S.; Hng, H.H.; Lou, X.W. Formation of Fe₂O₃ microboxes with hierarchical shell structures from metal-organic frameworks and their lithium storage properties. *J. Am. Chem. Soc.* 2012, 134, 17388–17391.

40. Zheng, F.; He, M.; Yang, Y.; Chen, Q. Nano electrochemical reactors of Fe₂O₃ nanoparticles embedded in shells of nitrogen-doped hollow carbon spheres as high-performance anodes for lithium-ion batteries. *Nanoscale* 2015, 7, 3410–3417.

41. Zhong, J.; Cao, C.; Liu, Y.; Li, Y.; Khan, W.S. Hollow core-shell η -Fe₂O₃ microspheres with excellent lithium-storage and gas-sensing properties. *Chem. Commun.* 2010, 46, 3869–3871.

42. Zhou, L.; Xu, H.; Zhang, H.; Yang, J.; Hartono, S.B.; Qian, K.; Zou, J.; Yu, C. Cheap and scalable synthesis of α -Fe₂O₃ multi-shelled hollow spheres as high-performance anode materials for lithium ion batteries. *Chem. Commun.* 2013, 49, 8695–8697.

43. Lin, H.B.; Rong, H.B.; Huang, W.Z.; Liao, Y.H.; Xing, L.D.; Xu, M.Q.; Li, X.P.; Li, W.S. Triple-shelled Mn₂O₃ hollow nanocubes: Force-induced synthesis and excellent performance as the anode in lithium-ion batteries. *J. Mater. Chem. A* 2014, 2, 14189–14194.

44. Ma, Y.; Ma, Y.; Geiger, D.; Kaiser, U.; Zhang, H.; Kim, G.T.; Diemant, T.; Behm, R.J.; Varzi, A.; Passerini, S. ZnO/ZnFe₂O₄/N-doped C micro-polyhedrons with hierarchical hollow structure as high-performance anodes for lithium-ion batteries. *Nano Energy* 2017, 42, 341–352.

45. Seng, K.H.; Li, L.; Chen, D.P.; Chen, Z.X.; Wang, X.L.; Liu, H.K.; Guo, Z.P. The effects of FEC (fluoroethylene carbonate) electrolyte additive on the lithium storage properties of NiO (nickel oxide) nanocuboids. *Energy* 2013, 58, 707–713.
46. Wu, L.; Buchholz, D.; Bresser, D.; Gomes Chagas, L.; Passerini, S. Anatase TiO₂ nanoparticles for high power sodium-ion anodes. *J. Power Sources* 2014, 251, 379–385.
47. Li, J.; Yan, D.; Hou, S.; Lu, T.; Yao, Y.; Chua, D.H.C.; Pan, L. Metal-organic frameworks derived yolk-shell ZnO/NiO microspheres as high-performance anode materials for lithium-ion batteries. *Chem. Eng. J.* 2018, 335, 579–589.
48. Zhao, Y.; Huang, G.; Li, Y.; Edy, R.; Gao, P.; Tang, H.; Bao, Z.; Mei, Y. Three-dimensional carbon/ZnO nanomembrane foam as an anode for lithium-ion battery with long-life and high areal capacity. *J. Mater. Chem. A* 2018, 6, 7227–7235.

Retrieved from <https://encyclopedia.pub/entry/history/show/31067>